APPLIED ECOLOGY

Full in vivo characterization of carbonate chemistry at the site of calcification in corals

Duygu S. Sevilgen[1]*, Alexander A. Venn[1], Marian Y. Hu[2], Eric Tambutté[1], Dirk de Beer[3], Víctor Planas-Bielsa[4,5], Sylvie Tambutté[1]*

Reef-building corals form their calcium carbonate skeletons within an extracellular calcifying medium (ECM). Despite the critical role of the ECM in coral calcification, ECM carbonate chemistry is poorly constrained in vivo, and full ECM carbonate chemistry has never been characterized based solely on direct in vivo measurements. Here, we measure pH_{ECM} in the growing edge of *Stylophora pistillata* by simultaneously using microsensors and the fluorescent dye SNARF-1, showing that, when measured at the same time and place, the results agree. We then conduct microscope-guided microsensor measurements of pH, $[Ca^{2+}]$, and $[CO_3^{2-}]$ in the ECM and, from this, determine $[DIC]_{ECM}$ and aragonite saturation state (Ω_{arag}), showing that all parameters are elevated with respect to the surrounding seawater. Our study provides the most complete in vivo characterization of ECM carbonate chemistry parameters in a coral species to date, pointing to the key role of calcium- and carbon-concentrating mechanisms in coral calcification.

INTRODUCTION

Coral calcification is the biomineralization process that involves the formation of calcium carbonate skeletons ($CaCO_3$), which form the massive bioconstructions of coral reefs. Although these ecosystems occupy only approximately 0.1% of the oceans' surface area, they are considered to be of major ecological and economic value (*1*). Coral reefs represent one of the most biodiverse habitats in the marine environment, harboring approximately one-third of the known marine species (*2*) and the highest density of animals to be found anywhere on the planet (*3*). They also provide an array of ecosystem services to many nations worldwide, including the protection of coasts from intense wave action in extreme weather scenarios (*4*, *5*).

The formation of the coral skeletons takes place in an extracellular calcifying medium (ECM), also referred to as calcifying fluid, subcalicoblastic medium, or subcalicoblastic space (*6*–*8*). The ECM is a semi-enclosed compartment of a few nano- to micrometers thickness that is "sandwiched" between the skeleton and the calcifying calicoblastic epithelium (CCE) (*9*). Together with three further overlaying epithelia, the CCE thus spatially separates the ECM from a direct contact with the surrounding environment (*9*). The chemical composition of the ECM is widely held to be an essential factor controlling calcification (*9*). Its importance in coral calcification and physiological resilience to environmental change has led to a large number of studies on relevant ECM parameters (pH, Ca^{2+}, and CO_3^{2-}, with the majority characterizing pH_{ECM} as a key parameter) and derived ECM carbonate chemistry [e.g., aragonite saturation state $\Omega_{arag} = [Ca^{2+}][CO_3^{2-}]/K_{sp}$ and dissolved inorganic carbon (DIC) concentration].

On the basis of all existing data, it is widely accepted that corals increase ECM pH and carbonate concentrations to elevate Ω_{arag} in the ECM above that of the surrounding seawater (*8*, *10*–*15*). Elevating Ω_{arag} in the ECM favors the formation of aragonite and is therefore thought to constitute a crucial step in the coral biomineralization process (*16*). This physiological process may also be crucial for corals and coral reef ecosystems to tolerate reduced seawater Ω_{arag} that will occur under ocean acidification (*11*, *14*, *17*). Furthermore, recent findings have shown that the up-regulation of Ca^{2+} in the ECM seems to be of notable importance for ECM carbonate chemistry and coral resilience (*14*) and assigns proper characterization of $[Ca^{2+}]$ a crucial role in coral biomineralization studies.

However, most of these findings come from indirect approaches using geochemical proxies rather than measurements in the ECM itself (boron isotope systematics for $\delta^{11}B$ and B/Ca, and Raman spectroscopy for Ω_{arag}) (*13*, *14*, *18*–*21*). Notably, few data come from direct in vivo measurements [confocal microscopy using the pH-sensitive fluorescent dyes SNARF-1 (carboxyseminaphthorhodafluor-1) and HPTS (8-hydroxypyrene-1,3,6-trisulfonic acid) or the application of microsensors for pH, Ca^{2+}, or CO_3^{2-} measurements] (*8*, *10*, *15*, *22*, *23*). Within the published in vivo studies, only the application of microsensors resulted in direct measurements of more than one parameter. The lack of multiparameter datasets from direct approaches is mainly due to the technical challenges in accessing the ECM in live corals and, in the case of confocal microscopy, the absence of carbonate and feasible calcium dyes. Microsensors, however, can be manufactured for all relevant ECM parameters, they are minimally invasive, and they measure on a scale of seconds and micrometers. However, although one microsensor study measured $[Ca^{2+}]$ (*10*) and one measured $[CO_3^{2-}]$ (*15*) in addition to pH_{ECM}, no study ever characterized all three parameters in a single study or species. This precludes a calculation of Ω_{arag} and a description of the full carbonate system based solely on direct measurements. A notable uncertainty of the available microsensor studies is that they leave the concern whether measurements were really conducted within the ECM, meaning that they were carried out in a "blind" manner. Thus, microsensor measurements were conducted after puncturing the coral coenosarc tissue to measure pH_{ECM} (*23*), making incisions with a scalpel (*10*) or inserting the sensor through the polyp mouth (*15*), without having an optical verification that the microelectrode was correctly placed in the ECM. This makes it difficult to rule out the influence of other compartments within the coral (e.g., the coelenteron).

The pH_{ECM} is the parameter for which most data are available in the literature obtained by all methods described. pH_{ECM} values range widely, with highest values generally obtained by microelectrode

[1]Centre Scientifique de Monaco, Marine Biology Department, 8 Quai Antoine 1er, MC 98000 Monaco, Monaco. [2]Christian-Albrechts-Universität zu Kiel, Hermann-Rodewald-Straße 5, DE 24118 Kiel, Germany. [3]Max Planck Institute for Marine Microbiology, Celsiusstr. 1, DE 28359 Bremen, Germany. [4]Centre Scientifique de Monaco, Polar Biology Department, 8 Quai Antoine 1er, MC 98000 Monaco, Monaco. [5]Laboratoire International Associé LIA 647 BioSensib (CSM-CNRS-Unistra), 8 Quai Antoine 1er, MC 98000 Monaco, Monaco.
*Corresponding author. Email: stambutte@centrescientifique.mc (S.T.); sevilgen@centrescientifique.mc (D.S.S.)

studies and lower values measured in boron and SNARF-1 studies. It is not known whether the different measurement techniques contribute to the range of pH values in the literature. Currently, no studies have attempted to combine the different techniques. Although Holcomb and colleagues (*24*) conducted boron and confocal measurements on the same coral sample, techniques were not combined for the different regions that were studied within the sample (apex, lateral region, and growing edge). To date, no studies have systematically compared the results of pH measurement using pH dyes and H^+-selective microelectrodes within the ECM.

In addition to this disparity of pH_{ECM} values in the literature, there is an ongoing debate over whether corals concentrate DIC in the ECM. While, based on several assumptions, isotope studies on *Porites* spp. indicated that [DIC] in the ECM can be two or more times higher than seawater (*13*, *21*), microelectrode work by Cai *et al.* (*15*) indicated that DIC in *Orbicella faveolata*, *Turbinaria reniformis*, and *Acropora millepora* is not elevated substantially above seawater values. This issue is important to resolve both from the standpoint of gaining a better mechanistic understanding of coral calcification and for the interpretation of geochemical isotope signatures (e.g., $\delta^{13}C$) widely used as paleoenvironmental records.

In this study, we performed microsensor investigations on the coral *Stylophora pistillata* to quantify the full carbonate system of the ECM based solely on direct in vivo measurements. We initially measured pH within the ECM of the growing edge of *S. pistillata* microcolonies by simultaneously using microsensors and the pH-sensitive dye SNARF-1. We then used microsensors to measure all three parameters (pH, $[CO_3^{2-}]$, and $[Ca^{2+}]$) within the ECM of the growing edge of the same coral species. Each parameter was measured in the light and in the dark, and correct placement of the microsensor tip within the ECM of the growing edge was optically verified by means of inverted microscopy. These data were then used to calculate ECM total [DIC] and Ω_{arag}. Applying approaches similar to those of earlier studies (*15*), we also used microsensors to measure pH and CO_3^{2+} under the coral polyps.

Our study provides the most comprehensive in vivo characterization of ECM carbonate chemistry to date, revealing that corals elevate calcium, [DIC], and Ω_{arag} in the ECM, in addition to increasing pH_{ECM}. These findings strongly support biological regulation of ECM carbonate chemistry and highlight its crucial role in coral calcification.

RESULTS

Simultaneous measurements of SNARF-1 and pH liquid ion exchange microsensors

To validate the application of microsensors for investigations of ECM chemistry at the growing edge of coral microcolonies, we measured pH_{ECM} in *S. pistillata* microcolonies grown on coverslips by simultaneously using pH microsensors and confocal microscopy coupled with the fluorescent, pH-sensitive dye SNARF-1 (Fig. 1). Confocal microscopy enabled imaging of the ECM, which was in contact with aragonite crystals underlying the calicoblastic epithelium (*8*, *22*). After the insertion of the microsensor into the ECM (Fig. 1, A and B), pH values increased immediately, reaching a maximum of 0.51 pH units higher relative to seawater values. These values closely correspond with pH values obtained by confocal analysis of SNARF-1 (Fig. 1C). Microsensor and SNARF-1 pH measurements were in close agreement throughout the experimental time series (Fig. 1C), demonstrating that these two in vivo methods produce very similar

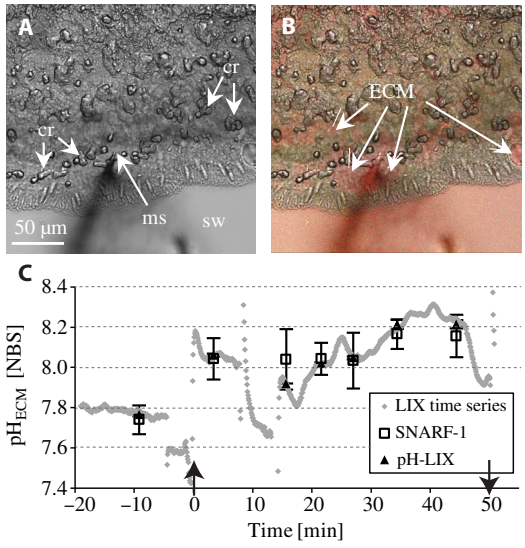

Fig. 1. Simultaneous measurements of pH in the ECM of the growing edge of a *S. pistillata* microcolony using a LIX microsensor and confocal microscopy with the pH-sensitive dye SNARF-1. (**A**) Inverted bright-field image showing the microsensor tip inside of the ECM. ms, microsensor; sw, seawater; cr, crystals. (**B**) Merged confocal and transmission image of the same area as shown in (A) with the tandem application of SNARF-1 (obtained at 585 ± 10 nm and 640 ± 10 nm) and the LIX microsensor. Green, cells; red, seawater and ECM. (**C**) ♦, time series of pH-LIX (acquisition time, 5 s); □, average ± SD $pH_{NBS,\ SNARF\text{-}1}$; ▲, average ± SD $pH_{NBS,\ LIX}$ obtained during the acquisition of SNARF-1 images; ↑, time of inserting the microsensor into the ECM at time point zero; ↓, time of retracting the microsensor out of the ECM. Data points between the arrows indicate measurements in the ECM, and data points before (negative time) are measurements in the seawater and the coral tissue before entering the ECM. Light conditions, 200 µmol photons cm^{-2} s^{-1}. No significant difference between microsensor and SNARF-1 pH measurements over the time series ($F_{1,12}$ = 1.50; P = 0.30).

results at the same location and time frame of measurement (Fig. 1C). The microsensor time series also show temporal pH dynamics within the ECM that commonly cannot be resolved by discontinuous measurements.

pH, $[CO_3^{2-}]$, and $[Ca^{2+}]$ in the ECM of the growing edge

Having made tandem measurements of pH_{ECM} using SNARF-1 and microsensor approaches to establish that microsensors could be reliably positioned in the ECM, we performed microsensor measurements in the growing edge. We attempted to perform simultaneous pH_{ECM} and $[CO_3^{2-}]$ readings using two microsensors; however, this frequently resulted in early tissue retraction or mesentery activity before values could stabilize (fig. S1). Thus, we separately measured pH, $[CO_3^{2-}]$, and $[Ca^{2+}]$ in the ECM at the growing edge of *S. pistillata* microcolonies using bright-field microscopy to position the electrode. Example measurements are shown in Fig. 2. Upon insertion of the microsensor into the ECM, we observed an immediate increase in all parameters measured as well as an immediate drop back to seawater values after retraction of the electrode from the colony. On average, pH was elevated by 0.44 pH units in the light and 0.43 pH units in the dark in the ECM relative to the surrounding seawater (Fig. 3 and Table 1). $[CO_3^{2-}]$ was elevated by 482 and 454 µmol kg^{-1} seawater and $[Ca^{2+}]$ by 2 mM relative to seawater in the light and dark (Fig. 3 and Table 1). A comparison of light and dark conditions (Fig. 3 and Table 1) revealed that there was no significant effect of light and dark

on all three parameters (pH_{ECM}: $P = 0.72$, $F_{1,20} = 0.13$; CO_3^{2-}: $P = 0.72$, $F_{1,6} = 0.15$; Ca^{2+}: $P = 0.78$, $F_{1,5} = 0.09$).

pH and CO_3^{2-} depth profiles on polyps

To investigate whether there are differences in pH and carbonate concentrations in the ECM, depending on the region of the coral microcolony studied (growing edge versus polyp), we also carried out microsensor measurements on coral polyps. The thickness of the coral skeleton under the polyps does not allow visualization of the ECM by bright-field or confocal microscopy and thus makes an optical verification of the position of the microelectrode in the ECM impossible.

During the microsensor measurements, external images of the coral polyp being measured were taken regularly throughout the experiment. The images revealed that, in most cases, the polyp frequently contracted after the insertion of the microsensor, often resulting in a full withdrawal of the polyp into the corallite calyx (Fig. 4B and fig. S2, A and B). Depth profiles of pH and carbonate were measured in the light (200 µmol photons m^{-2} s^{-1}) by starting measurements in the seawater above the polyp and entering it stepwise through the mouth and through the gastric cavity until the skeleton was reached (see Materials and Methods for further details).

In the overlaying seawater, pH remained constant at 8.06 ± 0.01 and increased to about pH 8.27 within the first millimeter of the polyp (Fig. 4A). With further advancement of the microsensor, values increased progressively until they reached a maximum of 8.92 ± 0.01 at the skeleton, displaying a Δ pH of 0.87 units to the ambient seawater (Fig. 4, A and C). In darkness, the pH immediately decreased (Fig. 4, A and C) to reach a dark pH minimum of 7.35 ± 0.01 after about 10 min. After reilluminating the sample, the pH immediately started to increase again, returning to original light values (8.88 ± 0.07) after about 20 min (Fig. 4, A and C). These findings suggest that photosynthesis and respiration exert a strong influence on the chemistry at the site of the microsensor measurements under the polyp during light and dark periods, contrasting with data obtained from measurements in the ECM of the growing edge.

To investigate the effect of photosynthesis on the observed pH increase, we exposed corals to DCMU [3-(3,4-dichlorophenyl)-1,1-dimethylurea], which specifically inhibits photosystem II and which instantly led to a drop in pH to 6.99 ± 0.02 (fig. S2A).

Depth profiles and light-dark shifts were also measured on polyps from the coral apex, where the influence of photosynthesis is expected to be less as they host almost no zooxanthellae (fig. S2B). In addition, measurements were also conducted on polyps containing zooxanthellae that naturally did not retract (fig. S2C). Data from polyps in apexes with low zooxanthellae abundance and from nonretracting polyps showed that the pH value at the skeleton was higher (pH 7.87 ± 0.05 and pH 7.65 ± 0.08, respectively) relative to values in the overlying tissues and gastric cavity (pH 7.21 ± 0.01 and pH 7.18 ± 0.04). However, these pH values did not exceed seawater pH (pH 7.92 ± 0.02 and pH 8.20 ± 0.02), and the values were not influenced by light-dark shifts (fig. S2B).

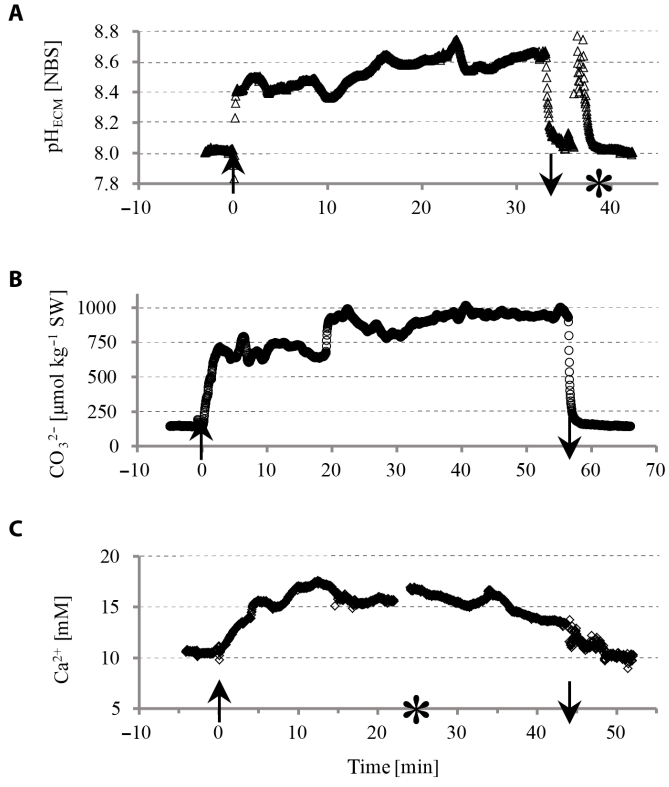

Fig. 2. Example time series and temporal dynamics of carbonate chemistry parameters measured with LIX microsensors in the ECM within the growing edge of *S. pistillata*. (**A**) pH, (**B**) CO_3^{2-}, (**C**) Ca^{2+}. Acquisition time, 2 s; illumination, 200 µmol photons m^{-1} s^{-1}; ↑ at time point zero, insertion of the microsensor into the ECM; ↓, time of retracting the microsensor out of the ECM; *, exchange of syringes of the perfusion system and resulting interference with the measurement setup.

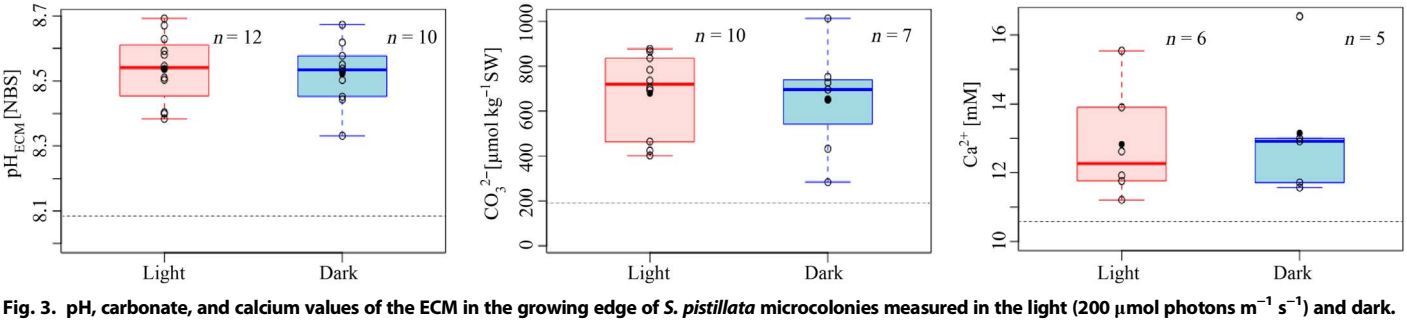

Fig. 3. pH, carbonate, and calcium values of the ECM in the growing edge of *S. pistillata* microcolonies measured in the light (200 µmol photons m^{-1} s^{-1}) and dark. Box and whisker plots show single replicate measurements (○); the mean (●); the first, second (median; bold line), and third quartile (horizontal lines of the boxes); and respective whiskers (vertical lines spanning to the lowest and highest data point of all data, excluding outliers). Replicate numbers (*n*) represent separate microcolonies and are given on each graph. Horizontal dashed line, seawater values (CO_3^{2-}, 196 ± 15 µmol kg^{-1} seawater; pH_{SW} [NBS], 8.09 ± 0.01; Ca^{2+}, 11 ± 0 mM).

Table 1. Carbonate chemistry parameters obtained in this study for seawater (SW) and the ECM of the growing edge of *S. pistillata* microcolonies in the light (200 µmol photons m^{-1} s^{-1}) and dark. Gray highlighted columns indicate parameters that were measured directly, and nonhighlighted columns show data derived from calculations (average ± SD).

	pH [NBS]	pH* [SWS]	CO_3^{2-} [µM kg^{-1} SW]	Ca^{2+} [mM]	DIC† [µmol kg^{-1} SW]	Ω_{arag}‡
Seawater	8.09 ± 0.01	7.93	196 ± 15	11 ± 0	2145 ± 279	2.9 ± 0.2
ECM						
Light	8.54 ± 0.10	8.38	679 ± 183	13 ± 2	3133 ± 1046	12.1 ± 3.6
Dark	8.52 ± 0.10	8.36	651 ± 235	13 ± 2	3084 ± 1269	11.9 ± 4.7

*pHSWS, pH NBS refitted after Dickson and Millero (*48*) (table 2). †Calculated according to Eq. 1 and based on pH_{SWS} (see Materials and Methods). ‡Calculated according to Eq. 2, $\Omega_{arag} = [Ca^{2+}][CO_3^{2-}]/K_{sp}$. K_{sp} = 7.184, as derived for salinity of 38 from Mucci (*53*) (solubility constants for aragonite are shown in table 4).

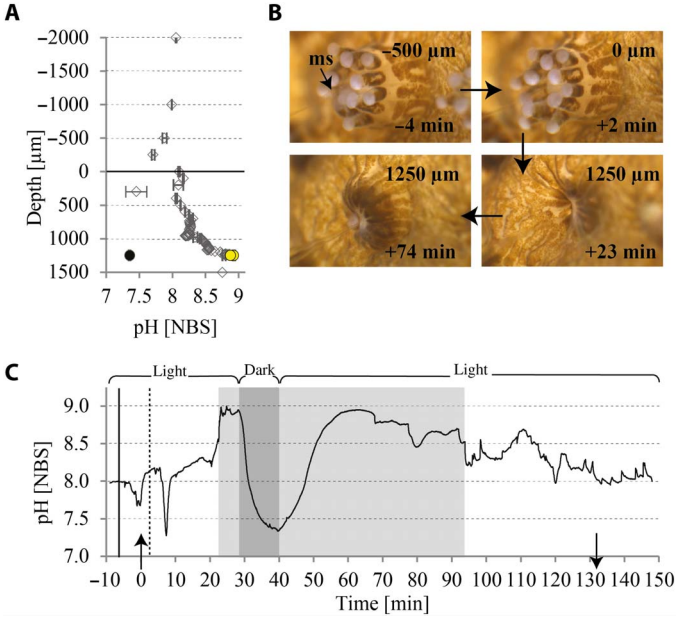

Fig. 4. pH measured by a LIX microsensor in a *S. pistillata* polyp with the sensor tip entered through the mouth. (**A**) pH depth profile (diamond symbols) corresponding to the time series in (C), showing maximum pH values in the light before and after a period of darkness (yellow circles) and a minimum value in darkness at the end of the dark period (black circle). The horizontal line indicates the top of the polyp mouth (0 µm). Negative depths represent measurements in the overlaying seawater; positive depths represent the inside of the polyp until the skeleton at 1250 µm. (**B**) Time series of pictures corresponding to (A) and (C) showing the coral polyp initially open (upper two images) and then retracted upon insertion of the microsensor (lower two images). (**C**) Time series of a coral pH profile (acquisition time every 2 s). Solid vertical line, seawater pH value at depth −2000 µm; dashed line indicates pH value at the entrance of the polyp mouth (0 µm); gray highlighted areas indicate measurements at the skeleton (1250 µm); dark gray area indicates period of darkness; ↑, time of reaching the polyp mouth; ↓, time of retracting the microsensor out of the polyp mouth.

Depth profiles of $[CO_3^{2-}]$ mirrored the results obtained by pH measurements in polyps containing zooxanthellae (fig. S3). During light conditions, $[CO_3^{2-}]$ increased progressively after entering the polyp until reaching maximum values at the skeleton of 654 ± 13 µM CO_3^{2-}. Upon switching off the light, values immediately started to drop, reaching a minimum of 41 ± 2 µM CO_3^{2-} in approximately 10 min. Switching the light back on and off a second time led essentially to the same values (645 ± 12 µM CO_3^{2-} and 49 ± 1 µM CO_3^{2-} for the second light and dark cycle, respectively). Corresponding images also showed a retraction of the polyp concurrently with the insertion of the sensor.

[DIC] and Ω_{arag} in the ECM at the growing edge

Results from the direct measurements of pH and $[CO_3^{2-}]$ under visual control were used to calculate ECM [DIC] according to Eq. 1 (see Materials and Methods and note S1). Carbonate concentrations were also used with the direct measurements of calcium concentrations to derive ECM Ω_{arag} (see Eq. 2 in Materials and Methods). We restricted calculations of both [DIC] and $[CO_3^{2-}]$ to data from the growing edge, where we had confirmed that microelectrodes could be correctly positioned in the ECM. Our DIC calculations revealed that [DIC] was, on average, elevated by 43 and 42% in the light and dark, respectively, as compared to seawater values (Table 1). The heterogeneity of the data resulted in pronounced variability resulting in minimum DIC concentrations close to seawater values and maximum DIC concentrations as high as approximately two times seawater DIC. Average values of Ω_{arag} of nearly 12 in the light and dark were fourfold that of $\Omega_{seawater}$ (Table 1). Overall, when considering the SD, Ω_{arag} values ranged from 7 to 17 and 8 to 16 in the light and dark, respectively.

DISCUSSION

Research on the chemical composition of ECM and the functioning of the CCE is central to understanding how corals calcify. This is important for predicting the impact of environmental stressors on coral reefs and improving the interpretation of skeletal isotope signatures for paleoreconstruction. The present study on live *S. pistillata* microcolonies delivers a set of direct in vivo measurements of pH_{ECM}, Ca^{2+}, and CO_3^{2-} concentrations on the same species, with optical verification of placement of the microelectrode within the ECM of the growing edge, an area that exhibits numerous freshly deposited and growing crystals (*8*, *25*). Calculations derived from these measurements reveal the extent to which ECM Ω_{arag} and DIC are elevated above seawater values and resolve uncertainty about derivations of ECM Ω_{arag} and DIC from skeletal geochemical proxies.

Furthermore, our results from simultaneous use of pH microsensors and SNARF-1 show that when measured at the same time and in

the same spot, data obtained by these two methods are in good agreement (Fig. 1), clarifying differences between previous findings reported within the literature. This supports the use of microelectrodes in the current and future studies and highlights the utility of using microscopy to guide the correct positioning of the microsensor tip into the ECM.

Previous studies that have used microsensors have been conducted in a blind manner in the polyps or between polyps in the coenosarc (*10*, *15*), where microscopic imaging is impossible. In these studies, positioning of the microelectrode within the ECM was assumed from a change of the sensor signal or breaking of the sensor once reaching the skeleton. Here, we also conducted microelectrode measurements under the polyps and conclude that it was not possible to reliably interpret the ECM chemistry measured under coral polyps, respectively, without optical verification of the site of measurement. This is based on the following observations. Initially, our results showed that both pH and $[CO_3^{2-}]$ under the polyps increased under light conditions to well above seawater values, which is in accordance with previous findings (*15*). However, we additionally carried out dark measurements, which revealed a profound decrease in both parameters to levels far below seawater values. Because of missing data, a direct comparison with other dark pH_{ECM} measurements under polyps is not possible. However, the low values of dark pH_{ECM} under the polyps contrast with our ECM values from the growing edge. They also do not agree with higher values of pH_{ECM} obtained in darkness in previous studies on *Galaxea fascicularis* (microsensors) and *S. pistillata* (SNARF-1) (*8*, *10*). To test what factors could influence our measurements under the polyps, we inhibited photosynthesis with DCMU and additionally measured in polyps largely devoid of zooxanthellae at the apex of coral colonies, where calcification rates are high. In line with dark measurements, the pH values in these experiments also fell well below seawater values. This strongly suggests that initial observations of elevated pH values at the skeleton were strongly influenced by photosynthetic CO_2 consumption (elevating pH) and that low dark pH values were likely driven by respiratory CO_2 production. Our observations that polyps frequently retracted after insertion of the microelectrode further support this idea. We propose that polyp retraction leads to a microenvironment of compressed tissues and high zooxanthellae density, where the influence of photosynthesis and respiration on chemistry at the site of the microelectrode measurement is greatly augmented (fig. S4).

Furthermore, we performed pH measurements at the skeleton in polyps that contained zooxanthellae but stayed relaxed and did not retract into the corallite calyx (fig. S2C). The pH profile from the mouth toward the skeleton showed a decline in pH, which is in accordance with findings on pH dynamics in the coral coelenteron (*26*). At the skeleton, pH slightly increased; however, it remained below seawater pH values. This conflicts with all existing pH_{ECM} data on scleractinian corals and suggests that unaltered ECM chemistry was not captured.

Drawing general conclusions on ECM chemistry under the polyps and comparing it to ECM chemistry in other regions of the coral based on these data are nearly impossible. If we consider to be measuring within the ECM under the polyp, its chemistry can be influenced by photosynthesis and respiration, and it would be impossible to dissociate to which proportion these processes influence ECM chemistry. Furthermore, polyp contractions and retraction could also alter the local microenvironment and thus the ECM chemistry, and we cannot say whether coral contraction and retraction are induced or enhanced by the insertion of microsensors into the polyps. Thus, we cannot estimate how representative the chemistry measured under compressed tissue layers is as opposed to natural conditions. Furthermore, this links to the fact that entering the ECM through several (compressed) tissue layers would likely cause tissue damage that could lead to a mixing of fluids of different compartments. Arriving at the ECM without any local tissue damage causing mixing seems rather unlikely. Furthermore, it seems impossible to ascertain whether a blind positioning of the microelectrode into the ECM, which is suggested to be a few micrometers or less in thickness in *S. pistillata* (*6*, *8*), is possible. Thus, we restricted our measurements of pH, $[Ca^{2+}]$, and $[CO_3^{2-}]$ and our calculations of Ω_{arag} and [DIC] to data derived from the growing edge, where we could be confident that microelectrodes were correctly placed in the ECM.

Another important experimental constraint we encountered in the current study was related to the simultaneous use of more than one microelectrode. Simultaneous measurements of two or three parameters (pH, $[Ca^{2+}]$, and $[CO_3^{2-}]$) in the ECM are desirable for improving the accuracy of calculations of carbonate chemistry, DIC, and Ω_{arag}, because data come from the same time and site of measurement. However, when we measured pH and $[CO_3^{2-}]$ with two microsensors in the same location and at the same time, coral colonies showed an accelerated stress response. Accordingly, tissue retraction around the measured area and increased mesentery activity directed toward the sensor tips were frequently observed (fig. S1B). We therefore avoided using simultaneous measurements for determinations of ECM chemistry within this study.

Measurements of pH, $[Ca^{2+}]$, and $[CO_3^{2-}]$ performed in the ECM of the growing edge, and the calculations of DIC and Ω_{arag} based on these data, provide valuable information on the mechanisms involved in the control of ECM chemistry. In *S. pistillata*, all parameters are elevated in the ECM with respect to seawater values. This was the case for both light and dark conditions, which did not differ from each other. The growing edge is generally inhabited by few zooxanthellae, reducing effects of photosynthesis and respiration, and a previous pH study on *S. pistillata* supports the finding of similar values during light and dark conditions (*17*). Furthermore, given that the rather small number of replicate measurements in the present study scattered over a wide range, it is possible that the number of replicates was not sufficient to resolve a difference.

The supply of ions to the ECM and their removal is thought to be governed by either transcellular pathways (through the cells), paracellular pathways (between the cells), or a combination of the two (*7*). It is noteworthy that in the case of the transcellular pathway, ions can be concentrated against their electrochemical gradient, whereas in the case of the paracellular pathway, ions will equilibrate according to their gradient. Because we have measured increased $[Ca^{2+}]$ at the calcification front compared to that of seawater, our results indicate an involvement of a transcellular pathway for the accumulation of calcium. Elevation of $[Ca^{2+}]$ in the ECM has also been recently derived from Ω_{arag} for two coral species by indirect methods (*14*), pointing toward cellular mechanisms to modulate $[Ca^{2+}]_{ECM}$. Molecular data suggest that calcium enters the calicoblastic cells via a calcium channel (*27*) and is released to the ECM through a calcium adenosine triphosphatase (ATPase) [plasma membrane calcium ATPase (PMCA)] (*28*). In addition to these calcium transport mechanisms, recent findings propose that calcium could also be transported via vesicles to the site of calcification in *S. pistillata* (*29*).

Concerning pH regulation, our results confirm that protons are removed from the calcification front, which is reflected in an elevation of

pH_{ECM} compared to the surrounding seawater. This could be facilitated by the PMCA, which functions as a calcium/proton exchanger present on the membrane of the calicoblastic cells (*28*). Last, we measured that [CO_3^{2-}] is elevated within the ECM with respect to seawater and determined that [DIC] is also elevated above seawater values, corroborating previous research that, based on different techniques and assumptions, suggested a carbon concentration mechanism in the ECM (*13*, *18*, *19*, *21*). On the basis of the present data, the current study also strongly indicates that mechanisms of DIC concentration must influence ECM carbonate chemistry. On a mechanistic level, transport of DIC coming from the calicoblastic cells into the ECM could occur through the diffusion of metabolic CO_2 [from respiration (*12*, *30*, *31*) or the supply of bicarbonate by a transporter of the SLC4 family (*32*)]. The conversion of these DIC species into carbonate would then be facilitated by a favorable pH, as determined in this study.

Our data, demonstrating that pH, [Ca^{2+}], and [CO_3^{2-}] are elevated in the ECM when compared to seawater, also align well with Ussing chamber measurements performed on *S. pistillata* colonies (*33*). These show that the calicoblastic epithelium behaves as a tight epithelium with low paracellular permeability and with significant transcellular ion transport capacities. Even if a paracellular pathway also occurs (*34*) and although the relative contributions of the paracellular versus the transcellular pathways may be species specific (*12*), our findings underline the involvement of a transcellular ion concentration mechanism in the ECM of *S. pistillata*.

The thermodynamic force driving the formation of aragonite is described by Ω_{arag}, and as such, there is a pronounced interest in determining Ω_{arag} in the coral ECM. In previous studies, Ω_{arag} has been derived solely from pH and/or carbonate values, with assumed values of calcium concentration matching seawater values or from Raman spectroscopy (*8*, *13*, *14*, *18*, *19*). Here, Ω_{arag} can be calculated from direct measurements of [Ca^{2+}] and [CO_3^{2-}] under light and dark conditions, giving Ω_{arag} values of about 12 ± 4 for light and 12 ± 5 for dark, respectively. These values match well with estimates of Ω_{arag} for coral skeletons made by Raman spectroscopy with values of 12.3 ± 0.3 and ~11 ± 0.5 for JCp-1 *Porites* coral standard and *Acropora*, respectively (*35*), and an Ω_{arag} of about 11.5 and 12 for *Acropora yongei* and *Pocillopora damicornis*, respectively (*14*).

The observed saturation states are sufficient for the inorganic precipitation of aragonite crystals. However, it has been previously pointed out that predicted rates of aragonite precipitation under the conditions used here at an Ω_{arag} of about 12 would correspond to lower calcification rates than typically measured for *S. pistillata* (*35*). This discrepancy may be related to a potential underestimation of the true surface area of the growing skeleton, which is a highly complex and fine three-dimensional structure (*36*). Thus, calcification rates may be overestimated when normalized to surface areas that are underestimated (*35*). Furthermore, the coral biomineralization mechanism involves organic matrix molecules, which may reduce the free energy required for crystal nucleation, possibly facilitating calcification at lower Ω_{arag} values (*29*, *37*, *38*). All values presented in this study were derived for *S. pistillata* and may vary when studied in other species.

In conclusion, the current study presents in vivo measurements of [Ca^{2+}], [CO_3^{2-}], and pH in the coral ECM and the determination of ECM Ω_{arag} and [DIC] solely from direct measurements. Notably, we demonstrate that ECM [Ca^{2+}] is elevated relative to seawater, and as such, future models of ECM chemistry or energetic models of ion transport to the ECM should take this into account, rather than assuming that the ECM [Ca^{2+}] is equivalent to seawater.

Our findings highlight several avenues for future research. First, we observed substantial variation in the values of [Ca^{2+}], [CO_3^{2-}], and pH_{ECM}, indicating temporal and spatial variation of Ω_{arag} in the ECM. This might explain observations of heterogeneous calcification rates across the skeleton and during skeleton formation made by previous authors (*39*, *40*). Formation of centers of calcification has been proposed to require higher Ω_{arag}, whereas prolongation by growth of aragonitic fiber bundles occurs at lower Ω_{arag} (*41*). A second area of future research should examine our results in the context of recent findings in the field of coral biomineralization, indicating that the calcification process is initiated by amorphous calcium carbonate precursor phases in the form of nanoparticles (*29*, *38*). These are suggested to be deposited in microenvironments that are enriched in skeletal organic matrix and organic fibers and would not require highly elevated extracellular Ω_{arag}. Thus, the role of elevated saturation states in these biomineralization models needs to be defined. Third, future work is needed to develop tandem microelectrode imaging approaches, which can extend spatial characterization of ECM carbonate chemistry to other areas of the coral colony, such as under polyps in other parts of the skeleton. As the current study demonstrates, using microelectrodes in conjunction with microscopy to ensure proper placement of the sensor is of great importance. These avenues of future research and continued research investment into coral physiology, in general, will help improve our knowledge of the coral biomineralization process, which is key to a deeper understanding and better predictions of how and why coral calcification responds to environmental change.

MATERIALS AND METHODS

S. pistillata microcolonies

All experiments were conducted on microcolony samples derived from *S. pistillata* colonies maintained at the Centre Scientifique de Monaco. Microcolonies were grown laterally on glass coverslips by the lateral skeleton preparative assay (*8*, *25*, *42*). During experiments, samples were kept at a temperature of 25°C, a salinity of 38, and light intensities of approximately 200 and 0 μmol photons m^{-2} s^{-1} during light/dark manipulations (see below).

Microsensor construction

pH, CO_3^{2-}, and Ca^{2+} liquid ion exchange (LIX) microsensors were prepared as described previously (*43*–*46*), with the exception that the green glass tubing was replaced by glass capillary tubes (borosilicate; inner diameter, 1.2 mm; outer diameter, 1.5 mm; Hilgenberg), which were pulled on a DMZ Universal puller (Zeitz-Instruments) into micropipettes with tip diameters of 1 μm. In brief, the micropipette tips were silanized (*43*), backfilled with electrolyte {for H^+: 300 mM KCl, 50 mM $NaPO_4$, pH 7; for CO_3^{2-}: $Na_2B_4O_7 \times 10H_2O$ (19.1 g $liter^{-1}$) + 200 μM $CaCO_3$ adjusted with 0.1 N HCl and NaOH to pH 9 [see (*44*)]; and for Ca^{2+}: 200 mM KCl, 2 mM $CaCl_2 \times 2H_2O$}, and broke open under the microscope to tip diameters of 2 to 3 μm. Tips were then front-filled in two steps with H^+, CO_3^{2-}, or Ca^{2+} ionophore, respectively (H^+ ionophore III, CO_3^{2-} ionophore VII, and Ca ionophore II; Sigma-Aldrich), as described previously (*44*). The micropipette tips were then glued to the rest of the glass housing, and microsensors were left to dry for 2 to 6 hours before measurements.

Microsensor calibration

pH and CO_3^{2-} microsensors were calibrated with commercially available pH buffers (pH 7 and 9, Fluka) and in seawater that was adjusted

to pH 6.5 to 9.5 in 0.5 pH units [National Bureau of Standards (NBS) scale] by adding HCl and NaOH. Seawater pH (pH_{SW} [NBS]) was measured with a pH electrode (Mettler Toledo), which was calibrated with three commercially available pH NBS buffers (pH 4, 7, and 10; Fisher Chemical). For each pH step, subsamples were taken to determine total scale pH (*m*-cresol purple) and total alkalinity (A_T, by titration). When alkalinity measurements were not possible, an average of all alkalinity measurements was taken for these datasets. For CO_3^{2-} calibration, concentrations were calculated in CO2SYS v2.1 using the measured pH and A_T with constants by Mehrbach *et al.* (*47*) refitted by Dickson and Millero (*48*), $KHSO_4$ from Dickson, and total boron by Uppström (*49*). Ca^{2+} sensors were calibrated in NaCl-based buffers (490 mM NaCl, 54 mM $MgCl_2 \times 6H_2O$ and 10.5 mM KCl, 500-ml ultrapure water), with at least three concentrations from 1, 5, 10, and 20 mM $CaCl_2 \times 2H_2O$.

Microsensor measurements

Microsensors were mounted on a motorized micromanipulator (MUX2, PyroScience GmbH) and connected to custom-built millivolt meters (Max Planck Institute for Marine Microbiology, Bremen, Germany). Amplifier outputs were channeled through an interface (Dual Channel Reader DCR16, PyroScience GmbH) to a laptop for data acquisition and control of the micromanipulator using the software Profix (version 4.51; PyroScience GmbH). Simultaneous use of two microsensors was facilitated by a custom-built adapter and a twin clamp (MM-TC, PyroScience GmbH). With the exception of one experiment where microsensor signals were recorded every 5 s (see below), microsensor signals were recorded every 2 s.

Measurements in the growing edge of *S. pistillata* microcolonies combined with inverted bright-field and confocal microscopy

Access with pH, CO_3^{2-}, and Ca^{2+} microsensors into the ECM in the growing edge of *S. pistillata* microcolonies was enabled by means of inverted bright-field microscopy using a 16× or 40× oil immersion lens. In certain experiments, microsensor pH_{ECM} measurements were also enabled by simultaneous confocal imaging of the ECM using the cell-impermeant fluorescent pH dye SNARF-1 (Leica SP5 confocal laser scanning microscope) using the same objectives. During the experiments, temperature was held constant at 25°C using a temperature-controlled microscope stage (Temperable Insert P, PeCon) linked to a temperature control unit (Polystat 36, Fisher Scientific) and a temperature-controlled seawater perfusion system (Thermo Clamp-1, AutoMate Scientific). The renewal rate was set to an optimum of 50% per minute for 2.5-ml volume of seawater within the perfusion chamber containing a coral sample of approximately 1 cm^2 (*8*).

After the initial calibration within a perfusion chamber solely containing seawater of the different calibration pH, a perfusion chamber containing a microcolony sample was placed under the microscope. Initially, the microsensor tip was carefully advanced toward the glass slide in a region outside the coral microcolony until it touched the glass. This position was set as depth zero. The sensor tip was then moved upward by several hundred micrometers (negative depth in vertical depth profiles) to record seawater values. Then, a region of interest was identified in the coral [distinct areas of ECM where the calicoblastic cell layer was lifted a few micrometers above the glass slide (*8*)]. The microsensor was moved toward this region until the sensor tip penetrated through the tissue and reached the ECM. The insertion of the sensor tip into the ECM was verified both visually by means of microscopy (squeezing of the tissue layers with subsequent penetration of the tip and simultaneous relaxation of the tissue surrounding the microsensor tip) and by a sudden change in signal. Because of the rigidity of the tissue, the sensor tip had to be pushed through the tissue layers by applying multiple depth steps, leading to a slight bend in the sensor tip and a final depth of >0 μm (positive depth in vertical depth profiles). Once the microsensor tip was placed within the ECM, time series were recorded to monitor temporal dynamics. We aimed to record series of at least 30 min; however, this was not always possible because of either a retraction of the coral tissue laying bare the microsensor tip or mesentery activity close to the microsensor tip disabling clean measurements. As the sensor could not be set perpendicular toward the sample because of limitations of the setup but was rather oriented in an angle of approximately 30° to 45°, we point out that in the depth profiles presented here, increments do not represent absolute distances to the sample.

Measurements of pH, CO_3^{2-}, and Ca^{2+} were performed in both the light and dark. Initially, light-dark shift measurements with an interval of approximately 10 min were performed as done previously (*10*) but showed no change of signal between light and dark. Thus, light and dark values were acquired from entire time series measured at light intensities of approximately 200 μm photons m^{-2} s^{-1} (halogen lamp KLQ150, Bioblock Scientific) or 0 μmol photons m^{-2} s^{-1} (light meter LI-250A, LI-COR). For dark measurements, coral microcolonies were first dark-adapted for 30 to 60 min (*50*), after which the corals were briefly illuminated by the microscope's light source, while the microelectrode was positioned. Samples were then returned to darkness for 30 min or longer during which a time series of microelectrode readings was recorded. Mean values of pH_{ECM}, [CO_3^{2-}], and [Ca^{2+}] were obtained by the following procedure. The first 10 min of each time series was discarded to allow microelectrode readings to stabilize and to allow recovery of the tissue after insertion of the sensor. Data from the remaining time series were averaged for each replicate. Replicate pH, CO_3^{2-}, and Ca^{2+} concentrations were obtained in separate colonies and averaged (±SD) for final values as presented in Table 1. At the end of each time series, the microsensor was retracted, and seawater values and, when necessary and possible, a second calibration series were recorded, which allowed the correction of a potential sensor drift.

Fluorescent dye imaging (SNARF-1)

SNARF-1 (Invitrogen) is an extracellular long-wavelength fluorescent pH indicator whose emission spectrum undergoes a pH-dependent wavelength shift. SNARF-1 measurements were essentially conducted as described previously (*8*). In brief, SNARF-1 solutions were prepared in filtered seawater to a final concentration of 45 μM. A total of 2.5 ml was then added to the perfusion chamber containing a microcolony sample that was incubated with the dye for 15 min before measurements. The samples were excited at 543 nm, and fluorescence was monitored at two emission wavelengths (585 ± 10 nm and 640 ± 10 nm) for subsequent ratiometric analysis. Calibration was done by determining the ratio of SNARF-1 fluorescence in filtered seawater adjusted to pH 6.5 to 9.5 in 0.5-pH NBS unit steps. This was done in both dark and light conditions and as described previously (*8*).

Simultaneous SNARF-1 and pH microsensor measurements

For simultaneous pH measurements by SNARF-1 and a microsensor, microsensor data were recorded continuously every 5 s, and pH using SNARF-1 was measured punctually every 5 to 10 min. A more frequent acquisition of fluorescent dye images was not possible because

of the sensitivity of the coral to the laser and a related tissue retraction. Microsensor measurements were subsequently averaged for the specific time frames (110 s) of each SNARF-1 data acquisition.

Measurements under the polyps of *S. pistillata* microcolonies

To compare measurements within the ECM in different regions of the microcolony, pH and CO_3^{2-} were also measured under the coral polyps. For this, glass slides with microcolonies were placed in a temperature-controlled seawater bath (100 ml) under a Leica Z16 APO macroscope (Leica Microsystems) connected to a camera system and computer screen, allowing macroscopic online observations. To minimize the effects of a photosynthesis- or respiration-driven diffusive boundary layer over the colony, a gentle surface current (~2 cm/s) was applied by blowing air with an air pump through a bent Pasteur pipette along the water surface. After calibration, the microsensor was moved to the seawater bath containing the sample, and the tip was positioned above the polyp mouth. This depth was set as zero. Generally starting from 1000 µm above the mouth (negative depths), the sensor was moved toward the polyp and inserted through the mouth (depth zero) until it could not be advanced any further (presumably reaching the skeleton and referred to as measurements "at the skeleton" in the text; maximum positive depths in the profiles). Contact with the skeleton could not be verified directly but was defined as when either the microsensor tip started to bend or the glass slide with the colony was moved in the water bath. Profiles were recorded in the light (200 µmol photons m^{-2} s^{-1}) with a dark period of 10 min at maximum depth. After the dark period, the light was switched back on for 10 min before an upward profile was recorded until the sensor had reached its original position in the seawater again. Data from experiments during which the sensor tip broke were excluded from the data presented within this study (this also applies to measurements in the growing edge).

DCMU treatment

To investigate the influence of photosynthesis on the pH under coral polyps, we used DCMU (Sigma-Aldrich). For the experiments, coral microcolonies were exposed to a seawater solution containing 100 µM DCMU in 0.1% acetone, which was prepared from a DCMU stock in 100% acetone (*51*).

DIC and Ω_{arag} calculations

CO2SYS does not allow the determination of DIC concentrations by use of pH and A_T (or CO_3^{2-}). Thus, DIC was calculated as done previously (*15*) by using the measured CO_3^{2-} concentrations, pH, and the dissociation constants of carbonic acid in seawater K_1 and K_2 (*52*) according to the following equation [derivation of Eq. 1 given in note S1]

$$[DIC] = [CO_3^{2-}]([H^+]^2/(K_1K_2) + [H^+]/K_2 + 1) \quad (1)$$

For this, we used the average values for CO_3^{2-} and pH and propagated their individual SD into a compound SD (see below).

Using the measured Ca^{2+} and CO_3^{2-} data, Ω_{arag} was calculated according to Eq. 2

$$\Omega_{arag} = [Ca^{2+}][CO_3^{2-}]/K_{sp} \quad (2)$$

where K_{sp} = 7.184, as derived by linear regression for salinity 38 from the given salinities from Mucci (*53*) (solubility constants for aragonite at 25°C; table 4). The calculations of the compound SD for DIC and Ω_{arag} are described in note S2.

Statistics

Calibration curves and one-way analysis of variance (ANOVA) were established and carried out using the program Origin 2017 (version 94E). Box plots representing the single data points; the average; the first, second (median), and third quartile; and respective whiskers (vertical lines representing the minimum and maximum of all data, excluding outliers) were generated using the software "R" version 3.3.1 (*54*).

SUPPLEMENTARY MATERIALS

Supplementary material for this article is available at http://advances.sciencemag.org/cgi/content/full/5/1/eaau7447/DC1

Fig. S1. Simultaneous measurement of pH and carbonate by two LIX microsensors in the same location (distance between sensor tips, <10 µm) of the ECM within the growing edge of a *S. pistillata* microcolony.

Fig. S2. pH profiles measured in the polyps of different microcolonies of *S. pistillata* by entering a pH LIX microsensor through the polyp mouth (≈0 µm).

Fig. S3. Carbonate depth profile measured by entering a CO_3^{2-} LIX microsensor through the polyp mouth (at ~200 µm) of a *S. pistillata* microcolony.

Fig. S4. Retraction of the coral polyp upon microsensor insertion.

Note S1. Derivation of Eq. 1 to calculate DIC.

Note S2. Calculation of the compound SD for DIC and Ω_{arag}.

REFERENCES AND NOTES

1. O. Hoegh-Guldberg, *Reviving the Ocean Economy: The Case for Action* (Geneva, 2015).
2. J. W. Porter, J. I. Tougas, in *Encyclopedia of Biodiversity*, S. A. Levin, Ed. (Elsevier, 2001) vol. 5, pp. 73–95.
3. M. D. Spalding, C. Ravilious, E. P. Green, *World Atlas of Coral Reefs* (University of California Press, 2001).
4. M. D. Spalding, B. E. Brown, Warm-water coral reefs and climate change. *Science* **350**, 769–771 (2015).
5. F. Ferrario, M. W. Beck, C. D. Storlazzi, F. Micheli, C. C. Shepard, L. Airoldi, The effectiveness of coral reefs for coastal hazard risk reduction and adaptation. *Nat. Commun.* **5**, 3794 (2014).
6. E. Tambutté, D. Allemand, D. Zoccola, A. Meibom, S. Lotto, N. Caminiti, S. Tambutté, Observations of the tissue-skeleton interface in the scleractinian coral *Stylophora pistillata*. *Coral Reefs* **26**, 517–529 (2007).
7. D. Allemand, É. Tambutté, D. Zoccola, S. Tambutté, Coral calcification, cells to reefs, in *Coral Reefs: An Ecosystem in Transition*, Z. Dubinsky, N. Stambler, Eds. (Springer Netherlands, 2011), vol. 3, pp. 119–150.
8. A. Venn, E. Tambutté, M. Holcomb, D. Allemand, S. Tambutté, Live tissue imaging shows reef corals elevate pH under their calcifying tissue relative to seawater. *PLOS ONE* **6**, e20013 (2011).
9. S. Tambutté, M. Holcomb, C. Ferrier-Pagès, S. Reynaud, É. Tambutté, D. Zoccola, D. Allemanda, Coral biomineralization: From the gene to the environment. *J. Exp. Mar. Bio. Ecol.* **408**, 58–78 (2011).
10. F. A. Al-Horani, S. M. Al-Moghrabi, D. de Beer, The mechanism of calcification and its relation to photosynthesis and respiration in the scleractinian coral *Galaxea fascicularis*. *Mar. Biol.* **142**, 419–426 (2003).
11. M. McCulloch, J. Falter, J. Trotter, P. Montagna, Coral resilience to ocean acidification and global warming through pH up-regulation. *Nat. Clim. Chang.* **2**, 623–627 (2012).
12. S. Hohn, A. Merico, Modelling coral polyp calcification in relation to ocean acidification. *Biogeosciences* **9**, 4441–4454 (2012).
13. N. Allison, I. Cohen, A. A. Finch, J. Erez, A. W. Tudhope; Edinburgh Ion Microprobe Facility, Corals concentrate dissolved inorganic carbon to facilitate calcification. *Nat. Commun.* **5**, 5741 (2014).
14. T. M. DeCarlo, S. Comeau, C. E. Cornwall, M. T. McCulloch, Coral resistance to ocean acidification linked to increased calcium at the site of calcification. *Proc. Biol. Sci.* **285**, 20180564 (2018).
15. W. J. Cai, Y. Ma, B. M. Hopkinson, A. G. Grottoli, M. E. Warner, Q. Ding, X. Hu, X. Yuan, V. Schoepf, H. Xu, C. Han, T. F. Melman, K. D. Hoadley, D. T. Pettay, Y. Matsui, J. H. Baumann, S. Levas, Y. Ying, Y. Wang, Microelectrode characterization of coral daytime interior pH and carbonate chemistry. *Nat. Commun.* **7**, 11144 (2016).

16. H. Lowenstam, Minerals formed by organisms. *Science* **211**, 1126–1131 (1981).
17. E. Tambutté, A. A. Venn, M. Holcomb, N. Segonds, N. Techer, D. Zoccola, D. Allemand, S. Tambutté, Morphological plasticity of the coral skeleton under CO_2-driven seawater acidification. *Nat. Commun.* **6**, 7368 (2015).
18. N. Allison, Reconstructing coral calcification fluid dissolved inorganic carbon chemistry from skeletal boron: An exploration of potential controls on coral aragonite B/Ca. *Heliyon* **3**, e00387 (2017).
19. S. Comeau, C. E. Cornwall, M. T. McCulloch, Decoupling between the response of coral calcifying fluid pH and calcification to ocean acidification. *Sci. Rep.* **7**, 7573 (2017).
20. N. G. Hemming, G. N. Hanson, Boron isotopic composition and concentration in modern marine carbonates. *Geochim. Cosmochim. Acta* **56**, 537–543 (1992).
21. M. T. McCulloch, J. P. D'Olivo, J. Falter, M. Holcomb, J. A. Trotter, Coral calcification in a changing world and the interactive dynamics of pH and DIC upregulation. *Nat. Commun.* **8**, 15686 (2017).
22. Y. Ohno, A. Iguchi, C. Shinzato, M. Inoue, A. Suzuki, K. Sakai, T. Nakamura, An aposymbiotic primary coral polyp counteracts acidification by active pH regulation. *Sci. Rep.* **7**, 40324 (2017).
23. J. B. Ries, A physicochemical framework for interpreting the biological calcification response to CO_2-induced ocean acidification. *Geochim. Cosmochim. Acta* **75**, 4053–4064 (2011).
24. M. Holcomb, A. A. Venn, E. Tambutté, S. Tambutté, D. Allemand, J. Trotter, M. McCulloch, Coral calcifying fluid pH dictates response to ocean acidification. *Sci. Rep.* **4**, 5207 (2015).
25. M. Raz-Bahat, J. Erez, B. Rinkevich, In vivo light-microscopic documentation for primary calcification processes in the hermatypic coral *Stylophora pistillata*. *Cell Tissue Res.* **325**, 361–368 (2006).
26. X. Yuan, W.-J. Cai, C. Meile, B. M. Hopkinson, Q. Ding, V. Schoepf, M. E. Warner, K. D. Hoadley, B. Chen, S. Liu, H. Huang, Y. Ye, A. G. Grottoli, Quantitative interpretation of vertical profiles of calcium and pH in the coral coelenteron. *Mar. Chem.* **204**, 62–69 (2018).
27. D. Zoccola, E. Tambutté, F. Sénégas-Balas, J.-F. Michiels, J.-P. Failla, J. Jaubert, D. Allemand, Cloning of a calcium channel α1 subunit from the reef-building coral, *Stylophora pistillata*. *Gene* **227**, 157–167 (1999).
28. D. Zoccola, E. Tambutté, E. Kulhanek, S. Puverel, J.-C. Scimeca, D. Allemand, S. Tambutté, Molecular cloning and localization of a PMCA P-type calcium ATPase from the coral *Stylophora pistillata*. *Biochim. Biophys. Acta* **1663**, 117–126 (2004).
29. T. Mass, J. L. Drake, J. M. Heddleston, P. G. Falkowski, Nanoscale visualization of biomineral formation in coral proto-polyps. *Curr. Biol.* **27**, 3191–3196.e3 (2017).
30. P. Furla, I. Galgani, I. Durand, D. Allemand, Sources and mechanisms of inorganic carbon transport for coral calcification and photosynthesis. *J. Exp. Biol.* **203**, 3445–3457 (2000).
31. J. Erez, Vital effect on stable-isotope composition seen in foraminifera and coral skeletons. *Nature* **273**, 199–202 (1978).
32. D. Zoccola, P. Ganot, A. Bertucci, N. Caminiti-Segonds, N. Techer, C. R. Voolstra, M. Aranda, E. Tambutté, D. Allemand, J. R. Casey, S. Tambutté, Bicarbonate transporters in corals point towards a key step in the evolution of cnidarian calcification. *Sci. Rep.* **5**, 9983 (2015).
33. I. Taubner, F. Bohm, A. Eisenhauer, E. Tambutte, S. Tambutte, S. Moldzio, M. Bleich, An improved approach investigating epithelial ion transport in scleractinian corals. *Limnol. Oceanogr. Methods* **15**, 753–765 (2017).
34. E. Tambutte, S. Tambutté, N. Segonds, D. Zoccola, A. Venn, J. Erez, D. Allemand, Calcein labelling and electrophysiology: Insights on coral tissue permeability and calcification. *Proc. Biol. Sci.* **279**, 19–27 (2012).
35. T. M. DeCarlo, P. J. D'Olivo, T. Foster, M. Holcomb, T. Becker, T. M. McCulloch, Coral calcifying fluid aragonite saturation states derived from Raman spectroscopy. *Biogeosci. Discuss.* **14**, 5253–5269 (2017).
36. D. J. Barnes, Coral skeletons: An explanation of their growth and structure. *Science* **170**, 1305–1308 (1970).
37. D. R. Talham, Biomineralization: Principles and concepts in bioinorganic materials chemistry Stephen Mann. Oxford University Press, New York, 2001. *Cryst. Growth Des.* **2**, 675 (2002).
38. S. Von Euw, Q. Zhang, V. Manichev, N. Murali, J. Gross, L. C. Feldman, T. Gustafsson, C. Flach, R. Mendelsohn, P. G. Falkowski, Biological control of aragonite formation in stony corals. *Science* **356**, 933–938 (2017).
39. F. Houlbrèque, A. Meibom, J.-P. Cuif, J. Stolarski, Y. Marrocchi, C. Ferrier-Pagès, I. Domart-Coulon, R. B. Dunbar, Strontium-86 labeling experiments show spatially heterogeneous skeletal formation in the scleractinian coral *Porites porites*. *Geophys. Res. Lett.* **36**, L04604 (2009).
40. O. H. Shapiro, E. Kramarsky-Winter, A. R. Gavish, R. Stocker, A. Vardi, A coral-on-a-chip microfluidic platform enabling live-imaging microscopy of reef-building corals. *Nat. Commun.* **7**, 10860 (2016).
41. M. Holcomb, A. L. Cohen, R. I. Gabitov, J. L. Hutter, Compositional and morphological features of aragonite precipitated experimentally from seawater and biogenically by corals. *Geochim. Cosmochim. Acta* **73**, 4166–4179 (2009).
42. L. Muscatine, E. Tambutte, D. Allemand, Morphology of coral desmocytes, cells that anchor the calicoblastic epithelium to the skeleton. *Coral Reefs* **16**, 205–213 (1997).
43. A. Gieseke, D. de Beer, in *Molecular Microbial Ecology Manual*, G. A. Kowalchuk, F. J. de Bruijn, I. M. Head, A. J. Van der Zijpp, J. D. Elsas, Eds. (Springer Netherlands, ed. 2, 2008), pp. 3483–3514.
44. D. de Beer, A. Bissett, R. de Wit, H. Jonkers, S. Köhler-Rink, H. Nam, B. Hyo Kim, G. Eickert, M. Grinstain, A microsensor for carbonate ions suitable for microprofiling in freshwater and saline environments. *Limnol. Oceanogr. Methods.* **6**, 532–541 (2008).
45. D. de Beer, M. Kühl, N. Stambler, L. Vaki, A microsensor study of light enhanced Ca^{2+} uptake and photosynthesis in the reef-building hermatypic coral *Favia* sp. *Mar. Ecol. Prog. Ser.* **194**, 75–85 (2000).
46. D. de Beer, A. Glud, E. Epping, M. Kühl, A fast-responding CO_2 microelectrode for profiling sediments, microbial mats, and biofilms. *Limnol. Oceanogr.* **42**, 1590–1600 (1997).
47. C. Mehrbach, C. H. Culberson, J. E. Hawley, R. M. Pytkowicx, Measurement of the apparent dissociation constants of carbonic acid in seawater at atmospheric pressure1. *Limnol. Oceanogr.* **18**, 897–907 (1973).
48. A. G. Dickson, F. J. Millero, A comparison of the equilibrium constants for the dissociation of carbonic acid in seawater media. *Deep Sea Res. Part A Oceanogr. Res. Pap.* **34**, 1733–1743 (1987).
49. L. R. Uppström, The boron/chlorinity ratio of deep-sea water from the Pacific Ocean. *Deep Sea Res. Oceanogr. Abstr.* **21**, 161–162 (1974).
50. A. Moya, S. Tambutté, E. Tambutté, D. Zoccola, N. Caminiti, D. Allemand, Study of calcification during a daily cycle of the coral *Stylophora pistillata*: Implications for 'light-enhanced calcification'. *J. Exp. Biol.* **209**, 3413–3419 (2006).
51. J. Laurent, S. Tambutte, É. Tambutté, D. Allemand, A. Venn, The influence of photosynthesis on host intracellular pH in scleractinian corals. *J. Exp. Biol.* **216**, 1398–1404 (2013).
52. F. J. Millero, T. B. Graham, F. Huang, H. Bustos-Serrano, D. Pierrot, Dissociation constants of carbonic acid in seawater as a function of salinity and temperature. *Mar. Chem.* **100**, 80–94 (2006).
53. A. Mucci, The solubility of calcite and aragonite in seawater at various salinities, temperatures, and one atmosphere total pressure. *Am. J. Sci.* **283**, 780–799 (1983).
54. R Development Core Team, *R: A Language and Environment for Statistical Computing* (R Foundation for Statistical Computing, 2017); https://www.r-project.org/.

Acknowledgments: We are grateful to the electronics workshop and the technicians of the microsensor group at the Max Planck Institute for Marine Microbiology (Bremen, Germany) for their technical assistance. We are thankful to N. Techer, N. Caminiti Segonds, and D. Desgré (Centre Scientifique de Monaco, Monaco) for laboratory and coral culture assistance. We also thank M. Bleich (Institute of Physiology, Kiel University, Germany) for access to his laboratories and the micropipette puller, and constructive exchanges on the study. **Funding:** This research was funded by the Government of the Principality of Monaco. M.Y.H. was funded by the DFG Emmy Noether Programme HU 2611/1-1. **Author contributions:** D.S.S., A.A.V., and S.T. designed the research and wrote the manuscript. D.S.S. performed experiments and analyzed data. A.A.V. and M.Y.H. helped in performing research and analyzing data, contributed to the manuscript, and participated in scientific discussions of the findings. E.T. contributed tools and participated in scientific discussions of the findings. V.P.-B. contributed to data processing and statistical calculations and to the manuscript. D.d.B. contributed materials/tools, participated in scientific discussions of the findings, and contributed to the manuscript. **Competing interests:** The authors declare that they have no competing interests. **Data and materials availability:** All data needed to evaluate the conclusions in the paper are present in the paper and/or the Supplementary Materials. Additional data related to this paper may be requested from the authors.

Submitted 13 July 2018
Accepted 4 December 2018
Published 16 January 2019
10.1126/sciadv.aau7447

Citation: D. S. Sevilgen, A. A. Venn, M. Y. Hu, E. Tambutté, D. de Beer, V. Planas-Bielsa, S. Tambutté, Full in vivo characterization of carbonate chemistry at the site of calcification in corals. *Sci. Adv.* **5**, eaau7447 (2019).

Full in vivo characterization of carbonate chemistry at the site of calcification in corals

Duygu S. Sevilgen, Alexander A. Venn, Marian Y. Hu, Eric Tambutté, Dirk de Beer, Víctor Planas-Bielsa and Sylvie Tambutté

Sci Adv **5** (1), eaau7447.
DOI: 10.1126/sciadv.aau7447